ARTICLES SCIENCE CHINA Materials

mater.scichina.com link.springer.com

Published online 13 March 2020 | https://doi.org/10.1007/s40843-019-1253-8

Sci China Mater 2020, 63(5): 758–768

Mesoporous TiO_2 mixed crystals for photocatalytic pure water splitting

Lichao Wang[1,2], Zhaozhong Xiao[1,2], Ye Liu[3], Shuang Cao[2*], Zhi Ma[1*] and Lingyu Piao[2*]

ABSTRACT **Semiconductor mesoporous single crystals have attracted considerable attention due to the merits of excellent light absorption ability and large surface area for photocatalysis capability. However, most of the materials have a relative large size (~um), which can hardly suppress the recombination of photogenerated electrons and holes. In this work, we synthesized a series of nano mesoporous TiO_2 mixed crystals (brookite and rutile) with high carrier transfer efficiency, improved mass transfer and diffusion abilities, which are crucial for the outstanding photocatalytic performance. Meanwhile, the key factors in the growth process and mechanism of the mesoporous TiO_2 mixed crystals were addressed. With the assistance of Pt nanoparticles, H_2 and H_2O_2 production can be simultaneously achieved and the efficiencies can reach up to 9.46 ± 0.56 and 3.29 ± 1.28 μmol mg^{-1} h^{-1}, respectively. The H_2 evolution rate is 2.8-fold higher than that of the reported TiO_2 nanoparticle catalyst (3.34 μmol mg^{-1} h^{-1}). The excellent photocatalytic efficiency can be attributed to the special mixed crystal structure of the mesoporous TiO_2 crystals. This work provides new ideas and guidance for precise synthesis of nano mesoporous TiO_2 mixed crystals and enhancing their water splitting performance with high value-added products.**

Keywords: mesoporous TiO_2, mixed crystal, photocatalytic water splitting, hydrogen, hydrogen peroxide

INTRODUCTION

Mesoporous materials with large specific surface area, high porosity, adjustable structure and pore size distribution, have attracted extensive attention in various fields, such as photocatalysis, dye-sensitized solar cells, and lithium ion batteries [1]. TiO_2 mesoporous single crystals (MSCs) have been extensively applied in photocatalysis due to the merits of nontoxicity, stability and low cost [1–3]. So far, various methods for the synthesis of TiO_2 MSCs have been reported, including hydrothermal method [2,4–11], template method [12–20], self-assembly method [16,21,22] and sol-gel method [23–26]. Various TiO_2 MSCs possessing different morphologies, such as sphere [4,9,10,16,22,27], rodlike [13,19], cuboid [2,16,20,23], network [12,15], have been obtained. However, most of them were in micron scale [2,4,9,10,12,16,21,22,27] and more easily led to carrier recombination [20,28–30]. Nano TiO_2 MSCs possess the advantages of shorter carrier migration distance and more favorable mass transfer and diffusion conditions. Therefore, controllable synthesis of nano TiO_2 MSCs to promote the efficiencies of photogenerated charge separation, light absorption and increase the active sites is desired [31–33].

Up to now, most of the applied TiO_2 MSCs are anatase. Although they have strong reducing capacities, they are not suitable for pure water splitting due to the unsuitable depth of electron-trap. It has been confirmed that the photocatalytic activity of TiO_2 is related to the depth of electron-trap, and brookite has the suitable depth of electron-trap compared with anatase and rutile to photocatalyze water oxidation and reduction [34,35]. Therefore, brookite is a promising material to achieve photocatalytic pure water splitting. Furthermore, the mixed-phase TiO_2 possesses a higher photocatalytic performance than the single-phase TiO_2 due to the better electron separation ability [36–40]. In this work, brookite-rutile mixed-phase TiO_2 was chosen as the model material for discussion, which has improved charge se-

[1] School of Chemical Engineering and Technology, Tianjin University, Tianjin 300072, China
[2] CAS Key Laboratory of Standardization and Measurement for Nanotechnology, CAS Center for Excellence in Nanoscience, National Center for Nanoscience and Technology, Beijing 100190, China
[3] School of Metallurgy and Chemical Engineering, Jiangxi University of Science and Technology, Ganzhou 341000, China
* Corresponding authors (emails: caos@nanoctr.cn (Cao S); mazhi@tju.edu.cn (Ma Z); piaoly@nanoctr.cn (Piao L))

paration and photocatalytic ability due to its energy band structure and interfacial properties [41]. The nano mesoporous TiO_2 mixed crystals (brookite and rutile) in this work was prepared by a novel and simplified method for photocatalytic pure water splitting with high value-added H_2 and H_2O_2 as the products. The enhanced photocatalytic activity is due to its nanometer size, mesoporous structure and mixed crystal effect. This work provides a promising strategy for synthesizing mesoporous TiO_2 mixed crystals with excellent photocatalytic pure water splitting performance.

EXPERIMENTAL SECTION

Chemical materials

Hydrochloric acid (HCl), ethylalcohol, methanol, sodium hydroxide and titanium tetrachloride ($TiCl_4$) were purchased from Beijing Sinopharm Chemical Reagent Co., Ltd. H_2PtCl_6 and 3,3'-dimethyldiphenylamine were obtained from J&K Scientific Ltd. Titanium butoxide (TBT) was purchased from Shanghai Macklin Biochemical Co., Ltd. 420840-LUDOX® AS-40 colloidal silica was purchased from Aldrich.

Preparation of seeded templates

First, 300 μL of $TiCl_4$ aqueous solution (3 mol L^{-1}) was added into 30 mL of 22-nm colloidal silica with stirring in a 80°C water bath for 1 h. Then the mixture was transferred to an oven for drying at 80°C for 12 h and calcinated at 300°C for 2 h in a muffle.

Preparation of mesoporous TiO_2 mixed crystals

The mesoporous TiO_2 mixed crystals were prepared by a silica-templated hydrothermal method. First, 20 mL of deionized water was mixed with 20 mL of concentrated HCl and stirred for 5 min at room temperature. Then 800 μL of TBT was added into the mixture and stirred for 5 min, and 800 mg of seeded silica templates was added subsequently to the solution. Then, the reactor was transferred into a Teflon-lined stainless steel autoclave (200 mL-volume) and heated at 180°C for 12 h. After that, the silica templates were removed by sodium hydroxide solution (3 mol L^{-1}) at 80°C. Then the mesoporous TiO_2 mixed crystals were collected by centrifugation and washed with deionized water and ethanol twice, respectively, then dried at 80°C for 12 h. Pt nanoparticles (NPs) were loaded by an *in-situ* photo-deposition method in a methanol solution (3 mL of methanol and 20 mL of deionized water) with H_2PtCl_6 (1 wt% Pt in the sample) as the precursor. The suspension was centrifuged after 1 h of UV light irradiation and dried at 80°C for 12 h to remove the remaining methanol and water.

Photocatalytic reaction

The as-prepared Pt/TiO_2 hybrid (1 mg) was dispersed in 20 mL of deionized water in a sealed quartz reactor. The dissolved gas was removed by being purged with argon flow for 30 min, then the suspensions were irradiated with a 500 W Hg lamp under magnetic stirring at room temperature (25°C). The evolved H_2 in the gas phase was examined by a Techcomp gas chromatography (GC-7900) with a thermal conductivity detector (TCD), 5 Å molecular sieve columns and Ar carrier.

The H_2O_2 detection method

The hydrogen peroxide was determined in 2.0 mL of reaction suspension. A 0.5 mL-volume indicator (1% *o*-tolidine in 0.1 mol L^{-1} HCl) was added to the suspension and the mixture reacted for 10 min at room temperature. The color of the suspension turned to blue. Then 2.0 mL of HCl (1.0 mol L^{-1}) was added to the mixture, and the color turned to yellow immediately. After centrifugation, the absorption spectrum of the supernate was measured by a UV-vis spectrophotometer. The characteristic maximum at 438 nm of absorption spectrum belongs to 2-electron oxidized toluidine.

RESULTS AND DISCUSSION

Mesoporous structure not only provides a large surface area and pore volume, but also offers an improved channel for the transport of reactants and products [5,42]. The formation of mesoporous structure is related to many factors, such as hydrothermal temperature [9] and crystallization ion environment [22]. In this work, we adjusted these conditions to obtain the sample with mesoporous structure in nanoscale.

The silica template hydrothermal method is the most widely used method to synthesize mesoporous TiO_2 mixed crystals. In this work, a novel method was introduced by modifying the size of template and simplifying the step for seed growth. Fig. 1 illustrates the synthetic process of nano mesoporous TiO_2 mixed crystals. In step 1, the $TiCl_4$ and SiO_2 nanospheres were mixed and seeded by a simple gelation and sintering method rather than the complicated traditional method [18]. In step 2, the crystal grew in the silicon template under different conditions by varing the temperature, reaction time, concentrations of HCl and TBT. The silica template was etched with NaOH to obtain samples with good

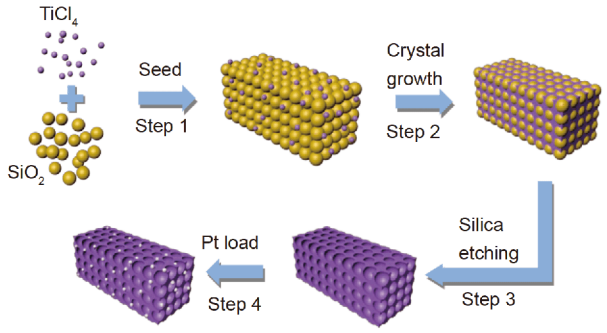

Figure 1 Schematic diagram of the synthesis process.

morphology preservation in step 3. Finally, the Pt NPs were loaded by *in-situ* photodeposition to obtain Pt/TiO_2 photocatalysts.

The key factors affecting the crystal phase and crystallinity

The performance of catalyst relates to many factors, such as crystallinity, surface area and surface properties [18,19]. The crystallization time, temperature and ionic environment significantly affect the crystallinity of materials. Fig. 2a shows the X-ray diffraction (XRD) patterns of mesoporous TiO_2 mixed crystals, according well with the standard brookite (JCPDS No. 29-1360) and rutile (JCPDS No. 21-1276). It is obvious that the crystallinity improves with prolonging reaction time. Brookite phase is the dominant product (~88%) with rutile phase accounting for a proportion of ~12% at 12 h (the calculation method is referred to Zhang *et al.* [43]). The crystallization process consists of the nucleation and crystal growth, and the products are poorly crystallized at the beginning of the reaction. After 2 h, the crystal begins to grow and tends toward stabilized crystallinity [44]. As shown in Fig. 2c, d, with the increase of hydrothermal temperature, the crystallinity of the sample becomes higher and the content of brookite becomes stable. The Raman spectra (Fig. S1a) are also consistent with the above results. The bands located at 153 and 332 cm^{-1} are assigned to brookite, and the bands located at 449 and 610 cm^{-1} are attributed to rutile [45–47]. Under sufficient reaction time, the relatively high temperature is conducive to improving the crystallinity of materials [9,44]. So, the reaction time and temperature are important factors for the crystallinity.

During the formation of TiO_2 crystal, the crystal phase

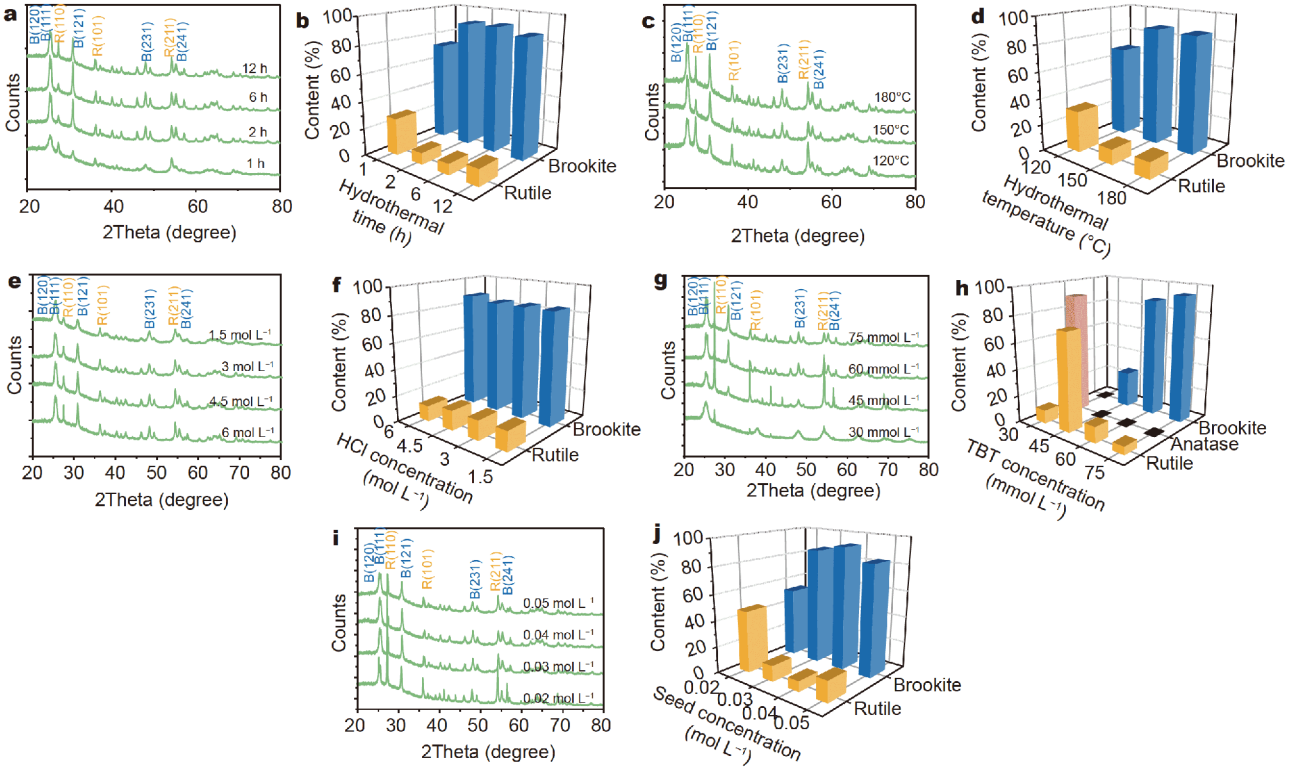

Figure 2 XRD patterns and contents of different crystal phases of the samples obtained at different hydrothermal times (a, b), hydrothermal temperatures (c, d), HCl concentrations (e, f), TBT concentrations (g, h), and seed concentrations (i, j).

has a direct relationship with the connection modes of $[TiO_6]$ octahedra precursors and the acidity greatly influences the number of shared edges of the $[TiO_6]$ octahedra by OH ligands. Rutile with two shared edges is easy to form at low pH, while anatase with four shared edges prefers to be obtained at a high pH value. A suitable pH value between them will facilitate the formation of brookite with three shared edges [39,41]. In this work, the pH of reaction media in silicon template is 9.1, which is suitable for the formation of brookite. However, the hydrolysis control agent out of silicon template is HCl, and therefore, in the initial reaction stage, the high concentration of HCl is beneficial to the formation of rutile [48]. The HCl concentration decreases in the silicon template as the reaction goes on and the proportion of brookite increases and stabilizes ultimately. Therefore, the pH value has a close relationship with the TiO_2 crystal phase.

Apart from that, the species and concentration of ions in the crystallization environment also have important impact on crystallinity [18,19]. Seen from the XRD patterns in Fig. 2e, g, and Raman spectra in Fig. S1b, c, with the increasing concentrations of HCl and TBT, the sample with high crystallinity can be obtained. It is proposed that the supersaturation of precursors has an effect on crystallization, and higher supersaturation is beneficial to crystal growth [49] because a high concentration of precursor can provide enough ions for the crystal growth. Notably, although the concentration of HCl has an influence on the crystallinity, it has no influence on the crystal phase (Fig. 2e, f). By contrast, the concentration of TBT has a great impact on the crystal phase. At low TBT concentration, the sample consisted of anatase and rutile, because only a small number of Ti^{4+} were involved in the formation of rutile. Meanwhile, the anatase was derived from the seed crystal encapsulated in the SiO_2 template. At this stage, brookite phase did not form. When the TBT concentration increased to 45 mmol L^{-1}, anatase phase disappeared and the sample consisted of brookite and rutile, with rutile as the main phase. Until the TBT concentration increased to 60 mmol L^{-1}, the brookite became the major phase. Because at the low TBT concentration, the concentration of Ti^{4+} diffused into templates was low and rutile could easily form at the shallow layer of the template. Only when the concentration of Ti^{4+} increased to a certain degree, the brookite could be obtained in the bulk of template. In addition, seed concentration also has a close relationship with the phase of the product. As shown in Fig. 2i, j, both lower and higher seed concentrations are conducive to the formation of rutile.

In conclusion, the reaction temperature and time not only affect the crystallinity of samples, but also significantly affect the formation of different crystal phases, just as the key ions (Ti^{4+}) do. With the appropriate hydrothermal temperature and reaction time, HCl and TBT control the supersaturation of the precursor to affect the crystal formation simultaneously.

The key factors affecting the morphology

The aspects for morphology optimization were discussed. Fig. 3 shows the growth of the sample with prolonging hydrothermal time. First, small NPs formed within ~1 h. As the crystallization time increased, mesoporous structures gradually formed in 2 h. Further prolonging to 12 h, the size reached about 320 nm with the morphology and size becoming stable. On the basis of dynamic balance and crystal growth theory, the crystallization process includes nucleation and crystal growth. The nucleus is firstly formed at the seed and with the time prolonging, the equilibrium state moves towards crystallization, and then the size of crystal gets larger [48,50]. After 1 h of reaction, the crystal just formed but did not have mesoporous morphology. The crystal growth during the period of 2-12 h enabled the crystal to obtain the complete mesoporous mixed crystal morphology with a larger size.

Hydrothermal temperature also has a significant effect

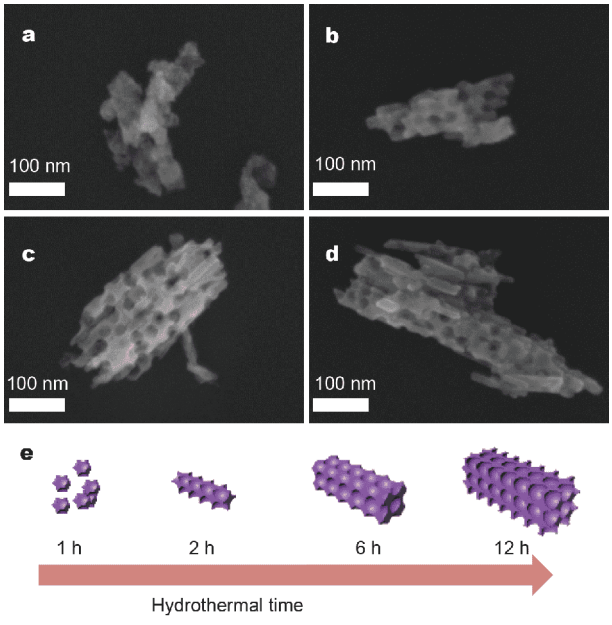

Figure 3 Scanning electron microscopy (SEM) images of the samples obtained at different hydrothermal times: (a) 1 h, (b) 2 h, (c) 6 h, (d) 12 h; (e) diagram of samples at different times.

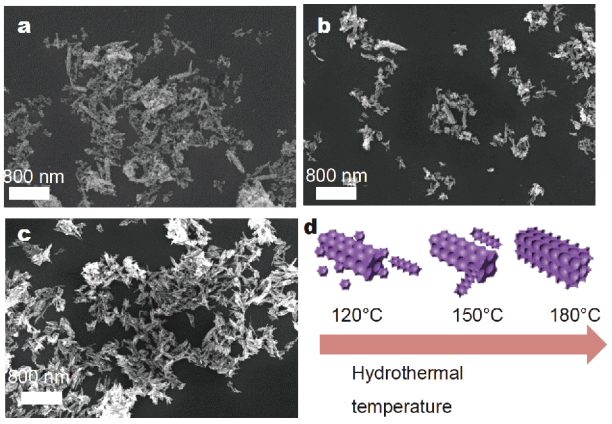

Figure 4 SEM images of the samples at various hydrothermal temperatures: (a) 120°C, (b) 150°C, (c) 180°C; (d) diagram of samples at various hydrothermal temperatures.

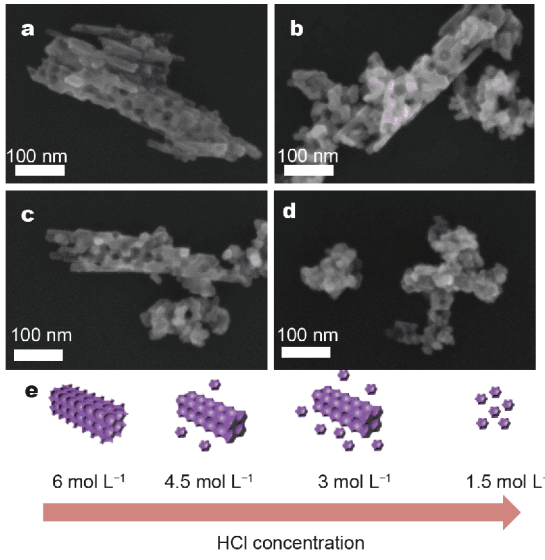

Figure 5 SEM images of the samples at a series of HCl concentrations: (a) 6 mol L^{-1}, (b) 4.5 mol L^{-1}, (c) 3 mol L^{-1}, (d) 1.5 mol L^{-1}; (e) diagram of samples at different HCl concentrations.

on the crystallization process. As shown in Fig. 4, some TiO_2 NPs were formed accompanied by mesoporous crystals at low temperature (120°C). When the temperature was raised up to 150°C, NPs disappeared and mesoporous fragments appeared. As the temperature continued to rise to 180°C, there were only mesoporous crystals. Therefore, the hydrothermal temperature affected both the crystallization rate and crystal size [18]. According to Arrhenius formula, the rate constant of hydrothermal reaction increases with temperature [50], and higher temperatures favor the formation of larger crystals [44]. So, some seeds just grow to particles or fragments at a low temperature. At higher temperature, faster crystallization rate enables the formation of larger size mesoporous crystals at a certain seed concentration and avoids the generation of particles or fragments. As a result, with the increasing temperature, the sample tends to be uniform.

The HCl concentration also has a great influence on the morphology. As shown in Fig. 5, at high concentration of HCl (6 mol L^{-1}), mesoporous crystals were obtained. With decreasing concentration of HCl, mesoporous structure gradually decreased, and NPs appeared. When the concentration of HCl decreased to 1.5 mol L^{-1}, mesoporous crystals were totally replaced by NPs. When the concentration of HCl increased to 7.5 and 9 mol L^{-1}, the samples did not show mesoporous morphology (Fig. S2c, d). These phenomena may be attributed to the effect of HCl on the hydrolysis rate of TBT. High concentration of HCl can slow down the hydrolysis rate of TBT to reduce the number of nuclei, resulting in larger crystals [51]. As the concentration of HCl decreases, the rate of hydrolysis of TBT increases and too many crystal nuclei form, leading to the formation of small particles.

The concentration of TBT has a positive correlation with the size of the crystals. Only NPs were obtained at a low concentration of TBT (30 mmol L^{-1}, Fig. 6 and Fig. S2a, b). When the concentration of TBT increased to 45 mmol L^{-1}, small size mesoporous fragments appeared. The complete MSCs were obtained when the concentration of TBT was above 60 mmol L^{-1}. High concentration

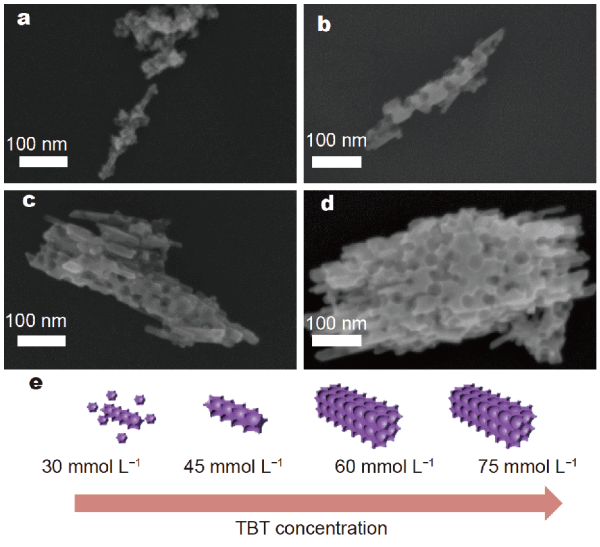

Figure 6 SEM images of the samples at different TBT concentrations: (a) 30 mmol L^{-1}, (b) 45 mmol L^{-1}, (c) 60 mmol L^{-1}, (d) 75 mmol L^{-1}; (e) diagram of samples at different TBT concentrations.

of precursor can effectively promote the nucleation and growth of crystals [52]. At low concentration of titanium source, there were no enough Ti^{4+} for the growth of complete morphology. And when the Ti^{4+} concentration reached to a certain value, the crystal morphology was not affected any more by increasing the concentration of TBT.

By contrast, seed concentration has a negative correlation with the size of the crystals. As shown in Fig. 7, at low seed concentration (0.01 mol L^{-1}), the large size mesoporous crystals can reach 1 μm in length. With the increase of seed concentration, the sizes of the crystals decrease and some fragments appear at the high seed concentration (0.05 mol L^{-1}). Therefore, the size of the mesoporous crystal is greatly affected by the template seed concentration. At a low seed concentration, there were plenty of space for crystal growth around the seed and enough Ti^{4+} were involved in the crystallization. With the increase of seed concentration and shrinking space caused by the steric hindrance effect, the size of the crystal decreased and the crystal growth space and the amount of Ti^{4+} were not enough to generate large mesoporous crystal, so that small size crystals and fragments were obtained. This result was consistent with previous report [18].

Fig. S3 shows the transmission electron microscopy (TEM) images of the samples synthesized with different conditions and high resolution TEM (HRTEM) images of mesoporous TiO_2 mixed crystals. The lattice spacing of

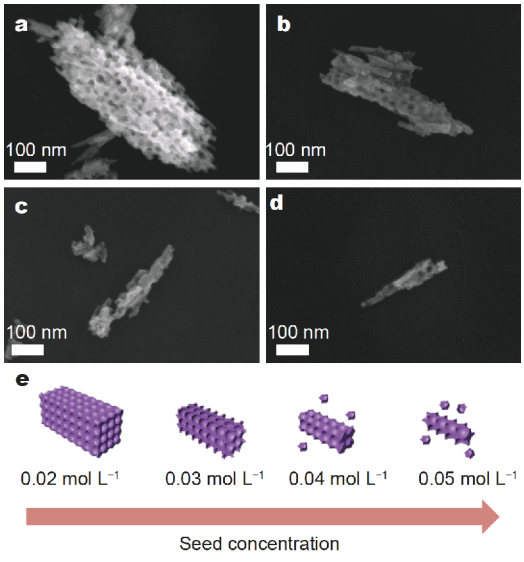

Figure 7 SEM images of the samples obtained at different seed concentrations: (a) 0.02 mol L^{-1}, (b) 0.03 mol L^{-1}, (c) 0.04 mol L^{-1}, (d) 0.05 mol L^{-1}; (e) diagram of samples at various seed concentrations.

0.347 and 0.325 nm can be ascribed to the brookite (111) and rutile (110) facets, respectively, [41,46,53–55], which proves that the materials are mixed crystals.

In conclusion, the mesoporous TiO_2 mixed crystals with better crystallization and complete morphology can be obtained at appropriate hydrothermal temperature, time, concentrations of crystal seed, HCl and TBT. Seed density controls the growth space of the crystal in the template. TBT provides the raw material for crystal growth, and HCl affects the nucleation and growth by controlling the rate of hydrolysis of TBT. The samples can be obtained with suitable size of growth space, adequate precursor and appropriate precursor hydrolysis rate.

The photoelectric and photocatalysis performances of the nano mesoporous TiO_2 mixed crystals

Based on the above analyses, we found that the reaction temperature, concentrations of HCl and TBT greatly affect the morphology and crystallization of the mesoporous TiO_2 mixed crystals. To evaluate their photocatalytic performances, selected materials were applied. As shown in the UV-vis absorption spectra (Fig. S4), all samples exhibit obvious absorbance in the UV region. The samples obtained at different temperatures and TBT concentrations show a similar absorbance, while the absorbance increases with the decreasing concentration of HCl. The observed band gap of the samples are between 2.80 and 2.95 eV, due to the influence of both phases of brookite and rutile and the samples' different particle sizes [41,46,56]. Effective separation of photogenerated electron hole pairs is the guarantee of high photocatalytic water splitting efficiency. Transient photocurrent test and electrochemical impedance spectroscopy (EIS) are common methods to characterize the charge separation and charge transfer efficiency of catalysts. The high photocurrent indicates an improved electron hole separation ability and the smaller radius in the Nyquist curve represents a better electron transfer efficiency [5,16,57]. As shown in Fig. 8a, b, all three samples show obvious transient photocurrent when the light is on, and the sample obtained at 150°C exhibits the highest current density at the beginning; however, it decays fast. By contrast, the sample synthesized at 180°C possesses the best charge separation and transfer ability, due to its good crystallinity and mesoporous morphology [58]. Fig. 8c, d shows the electrochemical properties of the samples obtained at different HCl concentrations. With the increase of HCl concentration, the current density increases and the impedance decreases, indicating better photoelectrochemical property. This relates to the good crystallinity

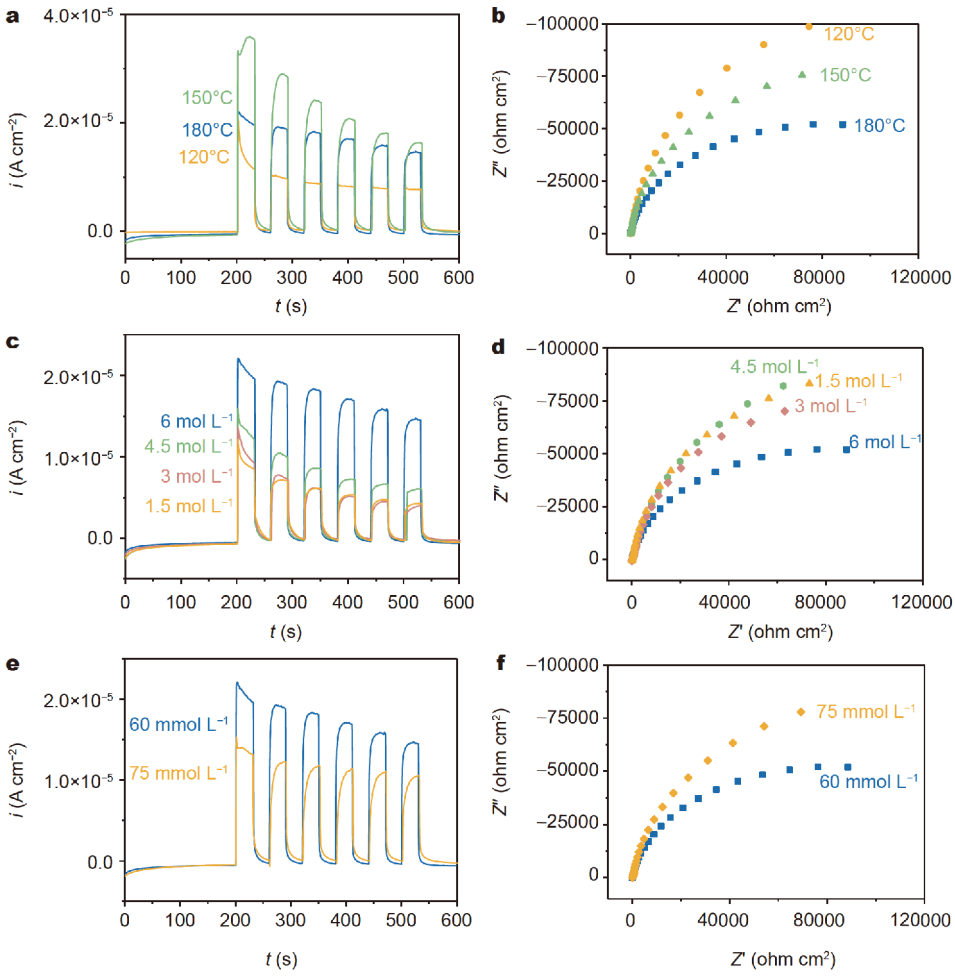

Figure 8 Transient photocurrent responses (a, c, e) and EIS spectra (b, d, f) of the samples obtained at different temperatures, HCl concentrations, and TBT concentrations, respectively.

and morphology of sample obtained at a high HCl concentration. As shown in Fig. 8e, f, the sample obtained at the TBT concentration of 60 mmol L^{-1} exhibits a better photoelectrochemical property. In conclusion, the samples with better crystallinity and morphology demonstrate better charge separation and transfer ability.

Fluorescence spectroscopy can reflect the transfer and separation ability of photon-generated carriers. Fig. S5 shows the photoluminescence (PL) spectra of the samples excited at 315 nm. With the temperature increasing, the fluorescence intensity is suppressed, and the sample synthesized with 60 mmol L^{-1} TBT and 6 mol L^{-1} HCl shows the lowest emission, suggesting the faster carrier transfer efficiency and efficient carrier separation ability [59], which is consistent with the photoelectrochemical results.

The photocatalytic pure water splitting performance and the effects of synthesis conditions on the activity of samples were evaluated based on the morphology, crystallization and photoelectric chemical properties. Pure water splits into H_2 and H_2O_2 in this system, and no oxygen is detected. The formation of H_2O_2 is due to the two-electron reaction of water oxidation, which has a kinetic advantage than the four-electron reaction [60–62]. Two ·OH radicals formed by water photo-oxidation dimerize into H_2O_2. So ·OH radical is the significant intermediate species in the photocatalytic oxidation reaction. As shown in Fig. S6, the electron spin resonance (ESR) results prove the formation of ·OH radicals with 5,5-dimethyl-1-pyrroline-*N*-oxide (DMPO) as the ·OH radical trap. The signal of DMPO-OH radical adduct (1:2:2:1, aN=aH=15.4G) was observed after 60 s UV light irradiation for the catalyst in pure water, illustrating the facilitated formation of ·OH radicals [60]. The X-ray

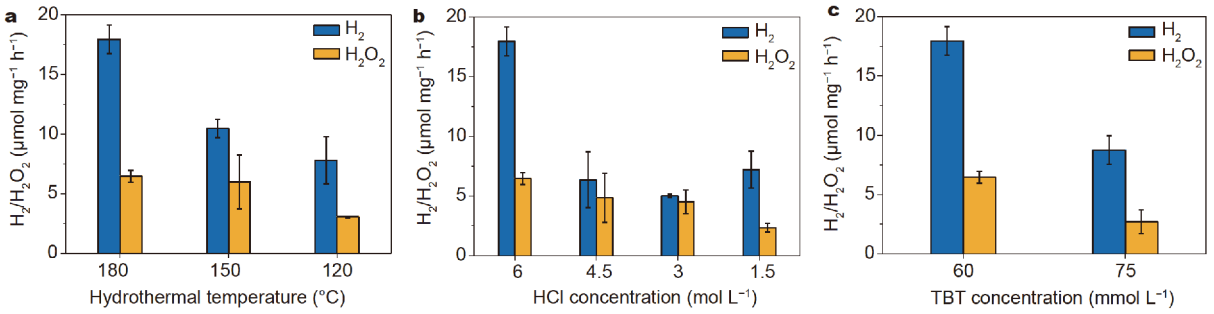

Figure 9 Photocatalytic activity of samples obtained at various hydrothermal temperatures (a), HCl concentrations (b), and TBT concentrations (c).

photoelectron spectroscopy (XPS) spectra further confirm the existence of abundant adsorbed –OH on the TiO_2 surface leading to the formation of ·OH radicals (Fig. S7). The peaks at 531.7 and 533.1 eV of O 1s indicated the amounts of –OH and physisorbed water on the surface of the sample, respectively. Both peaks increased for the sample with UV light irradiation, indicating that the Pt/TiO_2 had a modified hydrophilic surface and improved –OH amount after irradiation [60,63]. Based on the above analyses, H_2O_2 was formed by the two-electron transfer process ($2H_2O \rightarrow H_2 + H_2O_2$).

Samples synthesized at higher temperatures show a better performance of hydrogen production due to the good crystallinity, charge separation and transfer ability [5,44] (Fig. 9a). As shown in Fig. 9b, the hydrogen production rate of the sample synthesized at high HCl concentration (6 mol L^{-1}) is higher than others, because mesoporous morphology obtained with the high HCl concentration ensures the charge transfer ability, resulting in the high activity. Besides, the sample obtained with 60 mmol L^{-1} TBT concentration (Fig. 9c) has a higher activity than that with a higher TBT concentration, probably due to its proper mixed crystal ratio.

The N_2 adsorption-desorption isotherms and pore size distribution curves of the samples demonstrate that the sample synthesized under the condition of 180°C, 1.5 mol L^{-1} HCl and 60 mmol L^{-1} TBT possessses the largest surface area (94.924 m^2 g^{-1}) and the sample obtained at 180°C, 6 mol L^{-1} HCl and 60 mmol L^{-1} TBT takes the second place (Fig. S8). However, the latter exhibits the highest photocatalytic performance because both large surface area and good crystallinity improve the charge separate and transfer efficiency.

Under optimized conditions, the mesoporous TiO_2 mixed crystals with Pt NPs as a cocatalyst achieve a high H_2 evolution activity of 9.46 ± 0.56 μmol mg^{-1} h^{-1}, which is 2.8-fold higher than the highest TiO_2-based overall water splitting system ever reported (3.34 μmol g^{-1} h^{-1}) (Fig. S9a) [64]. And the rate of H_2O_2 production could reach 3.29 ± 1.28 μmol mg^{-1} h^{-1}. The increase of H_2O_2 is not obvious with the increase of irradiation time. It may be related to the adsorption of H_2O_2 on the surface of the catalyst. The system also exhibits an outstanding photocatalytic stability, which can maintain for more than 40 h (Fig. S9b). It is proposed that the excellent photocatalytic performance of mesoporous TiO_2 mixed crystals is related to the large surface area, porous structure and good crystallinity.

CONCLUSIONS

To improve the performance of TiO_2 in photocatalytic pure water splitting, nano scale mesoporous TiO_2 mixed crystals was firstly prepared in this paper. The synthetic protocol which affects the structures and properties of the materials is illustrated, including seed concentration, hydrothermal conditions and crystal growth environment. Appropriate crystallization time, reaction temperature and ionic concentratons are essential to obtain mesoporous TiO_2 mixed crystals with the high photocatalytic efficiency. Under optimized conditions, the H_2 and H_2O_2 production rates can reach up to 9.46 ± 0.56 and 3.29 ± 1.28 μmol mg^{-1} h^{-1}, respectively. The H_2 evolution rate is 2.8-fold higher than that of the reported TiO_2-based overall water splitting catalyst (3.34 μmol mg^{-1} h^{-1}). This work confirms that the photocatalytic performance can be enhanced by nano crystallization to improve the carrier transport efficiency, increase the reactivity surface and control the suitable conditions for mass transfer and diffusion.

Received 7 November 2019; accepted 15 January 2020; published online 13 March 2020

1 Bagheri S, Mohd Hir ZA, Yousefi AT, *et al.* Progress on mesoporous titanium dioxide: synthesis, modification and applications.

Microporous Mesoporous Mater, 2015, 218: 206–222
2 Dong Y, Fei X, Zhou Y. Synthesis and photocatalytic activity of mesoporous – (001) facets TiO_2 single crystals. Appl Surf Sci, 2017, 403: 662–669
3 Alagarasi A, Rajalakshmi PU, Shanthi K, *et al.* Ordered mesoporous nanocrystalline titania: a promising new class of photocatalyic materials. Catal Today, 2018, 309: 202–211
4 Zou M, Xiong F, Ganeshraja AS, *et al.* Visible light photocatalysts (Fe, N):TiO_2 from ammonothermally processed, solvothermal self-assembly derived Fe-TiO_2 mesoporous microspheres. Mater Chem Phys, 2017, 195: 259–267
5 Zhou Y, Fang W, Deng Y, *et al.* Enhanced photoreduction of Cr(VI) and photooxidation of NO over TiO_{2-x} mesoporous single crystals. RSC Adv, 2017, 7: 55927–55934
6 Fan Z, Meng F, Gong J, *et al.* One-step hydrothermal synthesis of mesoporous Ce-doped anatase TiO_2 nanoparticles with enhanced photocatalytic activity. J Mater Sci-Mater Electron, 2016, 27: 11866–11872
7 Lan K, Liu Y, Zhang W, *et al.* Uniform ordered two-dimensional mesoporous TiO_2 nanosheets from hydrothermal-induced solvent-confined monomicelle assembly. J Am Chem Soc, 2018, 140: 4135–4143
8 Jiao Y, Chen X, He F, *et al.* Simple preparation of uniformly distributed mesoporous Cr/TiO_2 microspheres for low-temperature catalytic combustion of chlorobenzene. Chem Eng J, 2019, 372: 107–117
9 Lu T, Wang Y, Wang Y, *et al.* Synthesis of mesoporous anatase TiO_2 sphere with high surface area and enhanced photocatalytic activity. J Mater Sci Tech, 2017, 33: 300–304
10 Wang L, Xie Y, Liu W, *et al.* Synthesis of mesoporous core-shell TiO_2 microstructures with coexposed {001}/{101} facets: enhanced intrinsic photocatalytic performance. Environ Sci Pollut Res, 2018, 25: 31250–31261
11 Jitputti J, Pavasupree S, Suzuki Y, *et al.* Synthesis and photocatalytic activity for water-splitting reaction of nanocrystalline mesoporous titania prepared by hydrothermal method. J Solid State Chem, 2007, 180: 1743–1749
12 Xie C, Yang S, Shi J, *et al.* Highly crystallized C-doped mesoporous anatase TiO_2 with visible light photocatalytic activity. Catalysts, 2016, 6: 117
13 Mohamed MA, Wan Salleh WN, Jaafar J, *et al.* Carbon as amorphous shell and interstitial dopant in mesoporous rutile TiO_2: Bio-template assisted sol-gel synthesis and photocatalytic activity. Appl Surf Sci, 2017, 393: 46–59
14 Wu T, Kang X, Kadi MW, *et al.* Enhanced photocatalytic hydrogen generation of mesoporous rutile TiO_2 single crystal with wholly exposed {111} facets. Chin J Catal, 2015, 36: 2103–2108
15 Xie C, Yang S, Li B, *et al.* C-doped mesoporous anatase TiO_2 comprising 10 nm crystallites. J Colloid Interface Sci, 2016, 476: 1–8
16 Yang Y, Li Y, Wang J, *et al.* Graphene-TiO_2 mesoporous spheres assembled by anatase and rutile nanowires for efficient NO photooxidation. J Alloys Compd, 2017, 699: 47–56
17 Zhang W, Zhou Y, Dong C, *et al.* Carbon-dot-modified TiO_{2-x} mesoporous single crystals with enhanced photocatalytic activity for degradation of phenol. Res Chem Intermed, 2018, 44: 4797–4807
18 Zheng X, Kuang Q, Yan K, *et al.* Mesoporous TiO_2 single crystals: facile shape-, size-, and phase-controlled growth and efficient photocatalytic performance. ACS Appl Mater Interfaces, 2013, 5: 11249–11257
19 Fang WQ, Huo Z, Liu P, *et al.* Fluorine-doped porous single-crystal rutile TiO_2 nanorods for enhancing photoelectrochemical water splitting. Chem Eur J, 2014, 20: 11439–11444
20 Zhou Y, Yi Q, Xing M, *et al.* Graphene modified mesoporous titania single crystals with controlled and selective photoredox surfaces. Chem Commun, 2016, 52: 1689–1692
21 Dörr TS, Deilmann L, Haselmann G, *et al.* Ordered mesoporous TiO_2 gyroids: effects of pore architecture and Nb-doping on photocatalytic hydrogen evolution under UV and visible irradiation. Adv Energy Mater, 2018, 8: 1802566
22 Zhang W, He H, Tian Y, *et al.* Synthesis of uniform ordered mesoporous TiO_2 microspheres with controllable phase junctions for efficient solar water splitting. Chem Sci, 2019, 10: 1664–1670
23 Lu J, Wang Y, Huang J, *et al. In situ* synthesis of mesoporous C-doped TiO_2 single crystal with oxygen vacancy and its enhanced sunlight photocatalytic properties. Dyes Pigments, 2017, 144: 203–211
24 Sreethawong T, Laehsalee S, Chavadej S. Comparative investigation of mesoporous- and non-mesoporous-assembled TiO_2 nanocrystals for photocatalytic H_2 production over N-doped TiO_2 under visible light irradiation. Int J Hydrogen Energy, 2008, 33: 5947–5957
25 Zhao Z, Xing Y, Li H, *et al.* Constructing CdS/Cd/doped TiO_2 Z-scheme type visible light photocatalyst for H_2 production. Sci China Mater, 2018, 61: 851–860
26 Likodimos V, Han C, Pelaez M, *et al.* Anion-doped TiO_2 nanocatalysts for water purification under visible light. Ind Eng Chem Res, 2013, 52: 13957–13964
27 Wang Y, Zhu Y, Yang X, *et al.* Plasmonic Au decorated single-crystal-like TiO_2-$NaYF_4$ mesoporous microspheres for enhanced broadband photocatalysis. Chin J Chem, 2017, 35: 949–956
28 Pan J, Liu G, Lu GQM, *et al.* On the true photoreactivity order of {001}, {010}, and {101} facets of anatase TiO_2 crystals. Angew Chem Int Ed, 2011, 50: 2133–2137
29 Fan Y, Hu G, Yu S, *et al.* Recent advances in TiO_2 nanoarrays/graphene for water treatment and energy conversion/storage. Sci China Mater, 2019, 62: 325–340
30 Ran J, Zhang J, Yu J, *et al.* Earth-abundant cocatalysts for semiconductor-based photocatalytic water splitting. Chem Soc Rev, 2014, 43: 7787–7812
31 Li D, Zhou H, Honma I. Design and synthesis of self-ordered mesoporous nanocomposite through controlled *in-situ* crystallization. Nat Mater, 2004, 3: 65–72
32 Kondo JN, Domen K. Crystallization of mesoporous metal oxides. Chem Mater, 2008, 20: 835–847
33 Jiao W, Xie Y, Chen R, *et al.* Synthesis of mesoporous single crystal rutile TiO_2 with improved photocatalytic and photoelectrochemical activities. Chem Commun, 2013, 49: 11770
34 Vequizo JJM, Matsunaga H, Ishiku T, *et al.* Trapping-induced enhancement of photocatalytic activity on brookite TiO_2 powders: comparison with anatase and rutile TiO_2 powders. ACS Catal, 2017, 7: 2644–2651
35 Moss B, Lim KK, Beltram A, *et al.* Comparing photoelectrochemical water oxidation, recombination kinetics and charge trapping in the three polymorphs of TiO_2. Sci Rep, 2017, 7: 2938
36 Di Paola A, Bellardita M, Palmisano L. Brookite, the least known TiO_2 photocatalyst. Catalysts, 2013, 3: 36–73
37 Monai M, Montini T, Fornasiero P. Brookite: Nothing new under the sun? Catalysts, 2017, 7: 304

38 Nobre FX, Gil Pessoa Junior WA, Ruiz YL, *et al.* Facile synthesis of nTiO_2 phase mixture: characterization and catalytic performance. Mater Res Bull, 2019, 109: 60–71
39 Yang Z, Wang B, Cui H, *et al.* Synthesis of crystal-controlled TiO_2 nanorods by a hydrothermal method: rutile and brookite as highly active photocatalysts. J Phys Chem C, 2015, 119: 16905–16912
40 Allen NS, Mahdjoub N, Vishnyakov V, *et al.* The effect of crystalline phase (anatase, brookite and rutile) and size on the photocatalytic activity of calcined polymorphic titanium dioxide (TiO_2). Polym Degradation Stability, 2018, 150: 31–36
41 Xu H, Zhang L. Controllable one-pot synthesis and enhanced photocatalytic activity of mixed-phase TiO_2 nanocrystals with tunable brookite/rutile ratios. J Phys Chem C, 2009, 113: 1785–1790
42 Lin J, Zhao L, Heo YU, *et al.* Mesoporous anatase single crystals for efficient $Co^{(2+/3+)}$-based dye-sensitized solar cells. Nano Energy, 2015, 11: 557–567
43 Zhang H, Banfield JF. Understanding polymorphic phase transformation behavior during growth of nanocrystalline aggregates: insights from TiO_2. J Phys Chem B, 2000, 104: 3481–3487
44 Mamaghani AH, Haghighat F, Lee CS. Systematic variation of preparation time, temperature, and pressure in hydrothermal synthesis of macro-/mesoporous TiO_2 for photocatalytic air treatment. J Photochem Photobiol A-Chem, 2019, 378: 156–170
45 Tompsett GA, Bowmaker GA, Cooney RP, *et al.* The Raman spectrum of brookite, TiO_2 (*Pbca*, $Z = 8$). J Raman Spectrosc, 1995, 26: 57–62
46 Cao Y, Li X, Bian Z, *et al.* Highly photocatalytic activity of brookite/rutile TiO_2 nanocrystals with semi-embedded structure. Appl Catal B-Environ, 2016, 180: 551–558
47 Bhattacharyya D, Kumar P, Smith YR, *et al.* Plasmonic-enhanced electrochemical detection of volatile biomarkers with gold functionalized TiO_2 nanotube arrays. J Mater Sci Tech, 2018, 34: 905–913
48 Byrappa K, Adschiri T. Hydrothermal technology for nanotechnology. Prog Cryst Growth Charact Mater, 2007, 53: 117–166
49 Rossetti Jr. GA, Watson DJ, Newnham RE, *et al.* Kinetics of the hydrothermal crystallization of the perovskite lead titanate. J Cryst Growth, 1992, 116: 251–259
50 Liu S, Zhou J, Liu R, *et al.* Preparation of nano ZrO_2 by integrated technique of high gravity field and microwave field. J Synth Cryst, 2014, 43: 79–86
51 Zhou W, Liu X, Cui J, *et al.* Control synthesis of rutile TiO_2 microspheres, nanoflowers, nanotrees and nanobelts *via* acid-hydrothermal method and their optical properties. CrystEngComm, 2011, 13: 4557
52 Li Y, Zhang M, Guo M, *et al.* Hydrothermal growth of well-aligned TiO_2 nanorod arrays: Dependence of morphology upon hydrothermal reaction conditions. Rare Met, 2010, 29: 286–291
53 Meng A, Zhang L, Cheng B, *et al.* Dual cocatalysts in TiO_2 photocatalysis. Adv Mater, 2019, 31: 1807660
54 Xiao F, Zhou W, Sun B, *et al.* Engineering oxygen vacancy on rutile TiO_2 for efficient electron-hole separation and high solar-driven photocatalytic hydrogen evolution. Sci China Mater, 2018, 61: 822–830
55 Testino A, Bellobono IR, Buscaglia V, *et al.* Optimizing the photocatalytic properties of hydrothermal TiO_2 by the control of phase composition and particle morphology. a systematic approach. J Am Chem Soc, 2007, 129: 3564–3575
56 Li C, Yang W, Li Q. TiO_2-based photocatalysts prepared by oxidation of TiN nanoparticles and their photocatalytic activities under visible light illumination. J Mater Sci Tech, 2018, 34: 969–975
57 Zhang W, Zhang H, Xu J, *et al.* 3D flower-like heterostructured TiO_2@$Ni(OH)_2$ microspheres for solar photocatalytic hydrogen production. Chin J Catal, 2019, 40: 320–325
58 Kinsinger NM, Wong A, Li D, *et al.* Nucleation and crystal growth of nanocrystalline anatase and rutile phase TiO_2 from a water-soluble precursor. Cryst Growth Des, 2010, 10: 5254–5261
59 Tang Y, Zhou P, Chao Y, *et al.* Face-to-face engineering of ultrathin Pd nanosheets on amorphous carbon nitride for efficient photocatalytic hydrogen production. Sci China Mater, 2019, 62: 351–358
60 Cao S, Chan TS, Lu YR, *et al.* Photocatalytic pure water splitting with high efficiency and value by Pt/porous brookite TiO_2 nanoflutes. Nano Energy, 2020, 67: 104287
61 Nakabayashi Y, Nishikawa M, Saito N, *et al.* Significance of hydroxyl radical in photoinduced oxygen evolution in water on monoclinic bismuth vanadate. J Phys Chem C, 2017, 121: 25624–25631
62 Seabold JA, Choi KS. Effect of a cobalt-based oxygen evolution catalyst on the stability and the selectivity of photo-oxidation reactions of a WO_3 photoanode. Chem Mater, 2011, 23: 1105–1112
63 Kumaravel V, Mathew S, Bartlett J, *et al.* Photocatalytic hydrogen production using metal doped TiO_2: A review of recent advances. Appl Catal B-Environ, 2019, 244: 1021–1064
64 Zhang W, Hu Y, Yan C, *et al.* Surface plasmon resonance enhanced direct *Z*-scheme TiO_2/ZnTe/Au nanocorncob heterojunctions for efficient photocatalytic overall water splitting. Nanoscale, 2019, 11: 9053–9060

Acknowledgements This work was financially supported by the National Natural Science Foundation of China (21703046), and the Ministry of Science and Technology of China (2016YFA0200902).

Author contributions Wang L designed and modified the samples and performed the experiments; Piao L and Cao S provided pivotal advice; Wang L wrote the paper with support from Piao L and Cao S. All authors contributed to the general discussion.

Conflict of interest The authors declare that they have no conflict of interest.

Supplementary information Supporting date are available in the online version of the paper.

Lichao Wang is currently a master student at the School of Chemical Engineering and Technology, Tianjin University. He joined the National Center for Nanoscience and Technology as a joint student. His research interests focus on the design and fabrication of photocatalysts for H_2 production.

Shuang Cao received her PhD degree from the Technical Institute of Physics and Chemistry, Chinese Academy of Sciences under the supervision of Prof. Yong Chen and Prof. Wen-Fu Fu in 2016. She joined the National Center for Nanoscience and Technology as a research associate in 2016. Her research focuses on designing and optimizing photocatalysts for H_2 production.

Lingyu Piao received her PhD degree from Tianjin University in 2002. She did her postdoctoral research at Peking University and Marie Curie University, respectively from 2002 to 2005. She joined the National Center for Nanoscience and Technology in 2005. Her research interest focuses on the design and synthesis of nano functional materials and their applications in energy, environmental photocatalysis and biology.

Zhi Ma is an associate professor of the School of Chemical Engineering and Technology, Tianjin University. He received his PhD degree from Tianjin University in 1998. He worked in Tianjin University after his master's degree in 1990. His research interest focuses on the application and exploitation aspects of nanometer catalyst.

介孔混晶TiO_2光催化全分解水研究

王利超[1,2], 肖召忠[1,2], 刘叶[3], 曹爽[2*], 马智[1*], 朴玲钰[2*]

摘要 半导体介孔单晶具有良好的光吸收能力和较大的比表面积, 因而受到广泛关注. 但多数材料的尺寸较大(~um), 难以抑制光电子与空穴的复合. 在本工作中, 我们准确地合成了一系列载流子转移效率高、传质和扩散能力强的纳米介孔板钛矿-金红石TiO_2混晶. 同时, 详细研究了介孔TiO_2混晶生长的关键因素和机理. 以Pt纳米颗粒作为助催化剂, 实现了全分解水产氢气和过氧化氢, 氢气和过氧化氢的生成速率分别达到9.46±0.56和3.29±1.28 μmol mg^{-1} h^{-1}. 氢气产率是目前报道的TiO_2(3.34 μmol mg^{-1} h^{-1})的2.8倍. 介孔TiO_2晶体的纳米尺度和混合晶体结构使其具有优异的光催化效率. 本工作为纳米介孔TiO_2混合晶体的精准合成, 以及光催化全分解水制备高附加值产品提供了新思路.